Photo or figure (optional)

Investigation of fracture toughening mechanisms of asphalt concrete using the clustered discrete element method

Hyunwook Kim, Empa, Road Eng./Sealing Components
William G. Buttlar, Univ. of Illinois at Urbana Champaign
Manfred N. Partl, Empa, Road Eng./Sealing Components

Conference paper STRC 2008

STRC

8th Swiss Transport Research Conference
Monte Verità / Ascona, October 15-17, 2008

Investigation of fracture toughening mechanisms of asphalt concrete using the clustered discrete element method

Hyunwook Kim
Empa
CH-8600, Dübendorf
Switzerland

Phone: 044-823-4474
Fax: 044-821-6244
email:hyunwook.kim@empa.ch

William G. Buttlar
Univ. of Illinois at Urbana-Champaign
61801 Urbana, USA

Phone: 1-217-333-5966
Fax: 1-217-333-1924
email: buttlar@uiuc.edu

Manfred N. Partl
Empa
CH-8600, Dübendorf
Switzerland

Phone: 044-823-4113
Fax: 044-821-6244
email:manfred.partl@empa.ch

October 2008

Abstract

Asphalt concrete is a quasi-brittle composite material which is composed of solid inclusions and a viscous matrix. The fracture of heterogeneous solids is a difficult problem to handle numerically due to the creation and continuous motion of new surfaces. A clustered discrete element method (DEM) is employed as a means to investigate fracture mechanisms in asphalt concrete at low temperatures. A bilinear cohesive softening model is implemented into the DEM framework to enable simulation of crack initiation and propagation in asphalt concrete. The meso-scale representation of the morphology of the material is incorporated into the DEM model using high-resolution imaging and image analysis software. The bulk properties and fracture parameters of multi-phase are obtained from experiments and calibration procedure. The two-dimensional clustered DEM method is applied into mode I fracture tests, e.g. disk-shaped compact tension (DC(T)) and single-edge notched beam (SE(B)) tests, to investigate various fracture mechanisms of asphalt concrete. The simulation results are shown to compare favourably with experimental results, and moreover, the simulations provide new insight into the fracture mechanisms in asphalt concrete. The modelling technique provides a physical description of the fracture process zone in laboratory fracture tests and the abilities to simulate mixed-mode fracture, crack competition, and distribution of macro- and micro-cracks.

Keywords

asphalt – fracture - discrete element method - cohesive softening model –DC(T) – SE(B)

1. Introduction

The fracturing of asphalt concrete paving surfaces and overlays is a significant cause of premature pavement deterioration. Cracks at the pavement surface create a permanent maintenance liability, and those which extend through the thickness of pavement reduce structural capacity and greatly increase pavement permeability and the intrusion of moisture into the pavement foundation. Asphalt concrete is a quasi-brittle composite material which is composed of solid inclusions (aggregates) and a viscous matrix (asphalt mastic). The mastic is composed of fine aggregates and asphalt binder and is the "glue" material holding larger aggregates together. The fracture of heterogeneous solids is a difficult problem to handle numerically due to the creation and continuous motion of new surfaces. The use of linear elastic fracture mechanics (LEFM) to analytically describe these mechanisms would be approximate, since the fracture patterns typically consist of a main crack, crack branching, secondary cracks, and microcracks.

However, there has been very limited work directed towards the development and/or application of models that can simulate the propagation of cracks in asphalt pavements while adequately considering the material's distinctive heterogeneity. Without the ability to model crack movement, it is not possible to properly assess crack initiation and the complexity of crack propagation. Typically, three general approaches can be employed in a research investigation, namely: experimental observations, analytical modeling, and numerical modeling. Experimental measurements can provide material properties and descriptions of material behavior, but the results may be affected by the boundary conditions, such as specimen size, geometry, and characteristics of the testing device. Analytical models can provide 'exact' answers and useful benchmark solutions, but are limited to relatively simple boundary value problems with highly idealized and simplified material properties. Numerical methods can be employed to extend analytical methods to consider more complex boundary conditions and material constitutive models, as has been demonstrated with the finite element method over the past several decades. However, modern numerical analysis techniques have the added advantage of allowing the study of the interaction between microstructural material properties and specimen geometry. For instance, information about the material structure at the meso-level can be incorporated into the numerical model, as shown in Figure 1.

Figure 1 Model calibration procedure with experimental and numerical methods

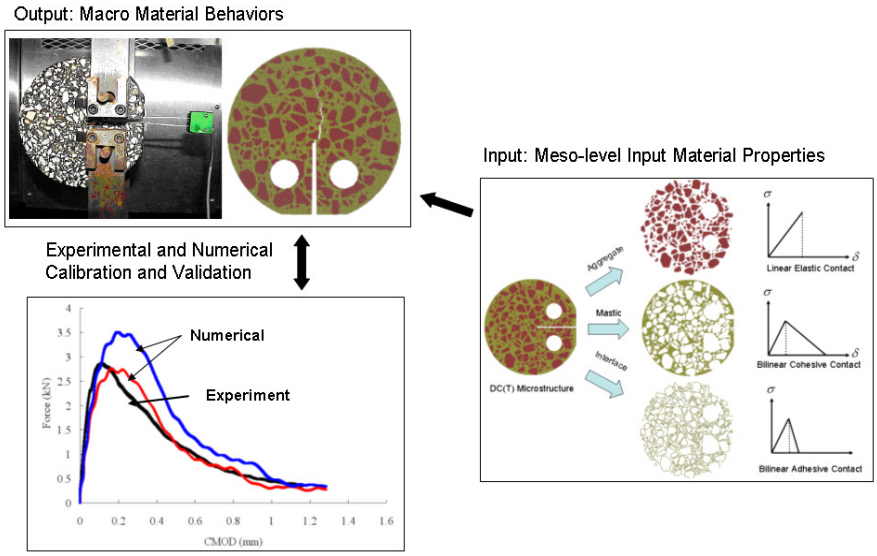

The main objective of this study is the initial step of a long-term project to investigate micromechanical fracture mechanisms in asphalt concrete using clustered discrete element method in conjunction with a high-resolution image technique. The long-term goal is the accurate prediction of laboratory and pavement fracture mechanisms and the development of design method to consider the fracture mechanisms of asphalt materials. However, due to time limitations, the integration of laboratory testing and numerical modeling is the focus of this study. The approach used herein incorporates experimental testing, multi-scale numerical simulation, image processing, and field performance. The micromechanical fracture modeling approach used can be viewed as an early developmental step towards the "virtual asphalt laboratory", where simulations of laboratory tests and eventually field response and distress predictions can be made to enhance our understanding of pavement distress mechanisms, such as thermal fracture or reflective cracking. The DEM will ultimately be used in multi-scale modeling, where global pavement response and local fracture behavior can be considered in the same numerical simulation.

2. Constitutive laws

2.1 Discrete element method

The discrete element method (DEM) originally developed by Cundall (1971) has proven to be a power and versatile numerical tool for modeling the behavior of granular and particulate systems, and also for studying the micromechanics of materials such as soil at the particle level. Also, the method has the potential to be an effective tool to model continuum problems, especially those that are characterized by a transformation from a continuum to discontinuum. The DEM discretizes a material using rigid elements of simple shape that interact with neighboring elements according to interaction laws that are applied at points of contact.

The analysis procedure consists of three major computational steps: *internal force evaluation*, in which contact forces are calculated; *integration of equations of motion*, in which element displacement are computed; and *contact detection*, where new contacts are identified and broken contacts are removed. In a DEM analysis, the interaction of the elements is treated as a dynamic process that alternates between the application of Newton's second law and the evaluation of a force-displacement law at the contacts. Newton's second law gives the acceleration of an element resulting from the force acting on it, including gravitational forces, external forces prescribed by boundary conditions, and internal forces developed at inter-element contacts. The acceleration is then integrated to obtain the velocity and displacement. The force-displacement law is used to find contact forces from known displacement. The equations of motion are integrated in time using the central difference method. The method can be computationally very demanding and thus, efficient algorithms, especially for the internal force evaluations and contact detection, must be used. Computational effectiveness will be particularly important for three-dimensional discretizations, the use of which is inevitable for obtaining fully realistic and accurate models for many applications. In the absence of damping, the DEM equilibrium equation at discrete time intervals for the system of particles is following:

Fehler! Es ist nicht möglich, durch die Bearbeitung von Feldfunktionen Objekte zu erstellen. (1)

Where, M is the mass matrix, a is the acceleration vector, K is the stiffness matrix, Δf is the incremental force vector, and Δx is the incremental displacement vector.

The translational and rotational stiffnesses of a particle relate increments of force and moment to increments of displacement and rotation via the matrix relations:

Fehler! Es ist nicht möglich, durch die Bearbeitung von Feldfunktionen Objekte zu erstellen. (2)

In a two-dimensional system, equation (2) can be expressed as:

Fehler! Es ist nicht möglich, durch die Bearbeitung von Feldfunktionen Objekte zu erstellen. (3)

The individual elements of this stiffness matrix can be expressed for a particular contact in terms of the particle radius r, the contact normal vector n_i, and the contact stiffnesses, i.e. K^n and K^s. Again, equation (2) can be expressed with the terms in a standard FE frame work from equation (4) to equation (7):

Fehler! Es ist nicht möglich, durch die Bearbeitung von Feldfunktionen Objekte zu erstellen. (4)

Fehler! Es ist nicht möglich, durch die Bearbeitung von Feldfunktionen Objekte zu erstellen. (5)

Fehler! Es ist nicht möglich, durch die Bearbeitung von Feldfunktionen Objekte zu erstellen. (6)

Fehler! Es ist nicht möglich, durch die Bearbeitung von Feldfunktionen Objekte zu erstellen. (7)

Where, $\{\Delta f\}$ are the incremental force vectors, $[K]$ is the contact stiffness matrix, $\{\delta u\}$ are the contact displacements, $\{\varepsilon\}$ are the contact strains, $\{\sigma\}$ are the contact stresses, $[B]$ is the strain matrix and $[D]$ is the elasticity matrix.

The elements of the stiffness matrix represent primarily the normal and shear springs that are present at the contact points. The stiffness matrix ($[K]$) changes during the analysis as contacts are formed and broken. Discrete element simulations can therefore be classified as non-linear, dynamic analyses. The principal difference between the available DEMs is the time integration algorithm used to solve equation (1) (O'Sullivan and Bray, 2001). Equation (2) is similar to the global equation considered in continuum finite element modeling.

The constitutive models used in the current two-dimensional (2-D) clustered DEM application consist of three parts: a contact stiffness model, a slip friction model and a bonding model. The linear contact model is defined by the normal and shear stiffness k_n and k_s (force/displacement) of the two contacting entities (ball-to-ball or ball-to-wall) acting in series. The contact normal secant and shear tangent stiffness are given by:

Normal secant stiffness:

Fehler! Es ist nicht möglich, durch die Bearbeitung von Feldfunktionen Objekte zu erstellen. (8)

Shear tangent stiffness:

Fehler! Es ist nicht möglich, durch die Bearbeitung von Feldfunktionen Objekte zu erstellen. (9)

The normal stiffness is a secant stiffness and it linearly relates the total normal force to the total normal displacement.

Fehler! Es ist nicht möglich, durch die Bearbeitung von Feldfunktionen Objekte zu erstellen. (10)

The shear stiffness is a tangent stiffness and it relates the increment of shear force to the increment of shear displacement.

Fehler! Es ist nicht möglich, durch die Bearbeitung von Feldfunktionen Objekte zu erstellen. (11)

The slip friction model is an intrinsic property of the two entities in contact (ball-to-ball or ball-to-wall) that governs frictional sliding of unbonded or debonded particles (ITASCA, 2002). The slip and bond models describe the constitutive behavior governing the response of particle contact points. The slip model is defined by the friction coefficient at the contact. For bonded assemblies, if the applied force becomes larger than the maximum allowable shear contact force, then slip is allowed to occur. The bond model allows particles to be joined at contacts, which activates material stiffness in opening and shear. The constitutive behavior for contact occurring at a point for the normal and shear components are given by Figure 2(a). S^n and S^s are normal and shear bond strengths; F^r is the frictional force. Figure 2(b) illustrates the calculation cycle. At the start of each time step, the set of contacts is

updated from the known particle and wall positions. The force-displacement law is then applied to each contact to update the contact forces based on the relative motion between the two entities at the contact and the contact constitutive model. Next, the law of motion is applied to each particle to update its velocity and position based on the resultant force and moment arising from the contact forces and any body forces acting on the particle. Also, the wall positions are updated based on the specified wall velocities.

Figure 2 Constitutive models and calculation cycle

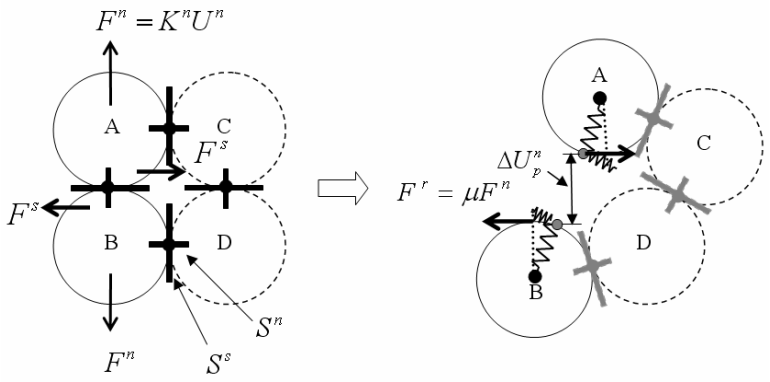

(a) Constitutive Contact, Slip, and Bond Model

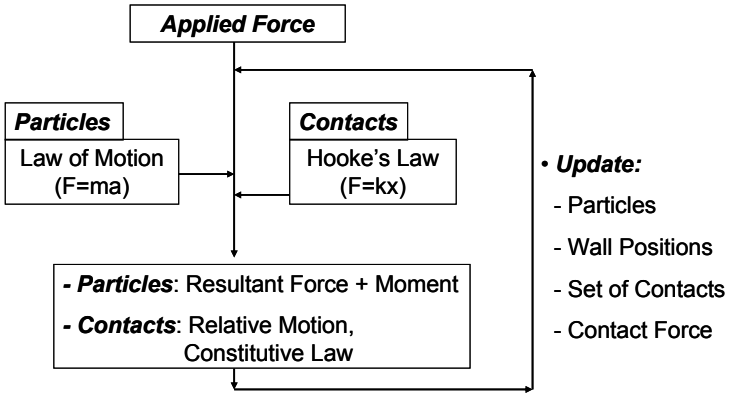

(b) Calculation Cycle of Discrete Element Method

2.2 Cohesive softening model

Dugdale (1960) and Barenblatt (1962) proposed cohesive models to investigate ductile and brittle material fracture behavior, respectively. The cohesive crack concept was later successfully extended by Hillerborg et al. (1976) to study nonlinear fracture processes in Portland cement concrete. Furthermore, cohesive zone models (CZMs) have been used to simulate the fracture process in a number of material systems under a variety of loading conditions (static, dynamic, cyclic, etc). The two most noteworthy cohesive failure models available in the literature are: the intrinsic potential-based model and extrinsic linear law model. In the intrinsic approach, the failure criterion is incorporated within the constitutive model of the cohesive elements. Failure is integrated into the cohesive law by increasing the cohesive tractions from zero to a failure point at which the tractions reach a maximum before gradually decreasing back to zero. In all intrinsic CZMs, the traction-separation relations for interfaces are such that with increasing interfacial separation, the traction across the interface reaches a maximum, then decreases and eventually vanishes, permitting a complete decohesion. The main difference between CZMs lies in the shape of the traction-displacement response. Bilinear CZMs can be described by two independent parameters. These parameters may be two of the three parameters, namely the cohesive energy Φ, and either of the cohesive strength σ_{max}, or the separation/critical length δ_{sep}.

Figure 3 Schematic concept of bilinear cohesive softening model

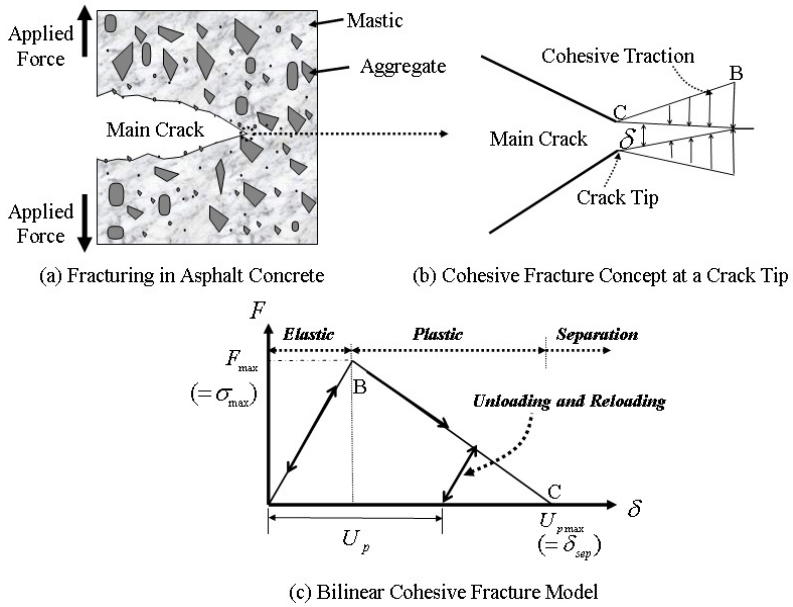

An intrinsic general cohesive softening model (CSM) is implemented as a user-defined model in the particle flow code (PFC-2D), which is in the form of a bilinear cohesive zone model (Figure 3(c)). In general, the cracking of asphalt concrete can occur in any weak point within the fracture process zone (Figure 3(a)) and the cohesive fracture concept at the crack tip can be simplified as shown in Figure 3(b). Geubelle et al. (1998) utilized a bilinear CZM to simulate spontaneous initiation and propagation of transverse matrix crack and delaminating fronts in thin composite plates subjected to low-velocity impact. In Figure 3(c), δ_{max} represents the location of cohesive crack tip and δ_{sep} is the complete material separation or the material crack tip, and σ_{max} is the normal cohesive strength. Point B represents the starting point of unrecoverable material degradation (or micro-crack initiation) and point C represents the condition where a crack face has fully separated and has released the energy potential associated with decohesion.

If the contact is in tension, the contact strength F_{max} is calculated from the two strength parameters (i.e. normal force, F^n_c and shear force, F^s_c) as a function of the current orientation of the contact force. It is assumed that contact strength varies as a linear function of the angle α:

$$F_{\max} = (1 - \frac{2\alpha}{\pi}) \times F_c^n + \frac{2\alpha}{\pi} \times F_c^s \tag{12}$$

Where, α is the angle between the directions of contact force and the line segment connecting the centers of particles. The yielding of bond in tension is determined by comparing the resultant contact force, i.e., with the contact strength.

$$F = \sqrt{(F^n)^2 + (F^s)^2} \tag{13}$$

The contact yields if the contact force is larger than the contact strength. In the present fracture modeling approach, Mode I (i.e., pure opening) fracture behaviors are dominant in both homogenous and heterogeneous specimen fracture simulations. However, unlike the homogenous mode I simulation where shear separations are negligible, in the heterogeneous material simulation, the meandering cracking activates a non-negligible amount of mixed-mode interface behavior (crack opening and sliding).

In the case of yielding of contact bonds, the increment of contact displacements, ΔU^k (k=n, s), can be decomposed into elastic and plastic contact displacement increments:

$$\Delta U^k = \Delta U_e^k + \Delta U_p^k \tag{14}$$

The force increment, ΔF^k, is a function of incremental elastic displacement only:

$$\Delta F^k = K^k \Delta U_e^k \tag{15}$$

Where,

$$\Delta U_e^k = \Delta U^k - \Delta U_p^k \tag{16}$$

The elastic (or plastic) displacement increment can be determined using the consistency condition (i.e., F - F_{max} = 0). In the softening portion of the model, the contact strength is a function of the accumulated plastic deformation, as described by:

$$F_c^k (U_p / U_{p\max}) = F_c^k (1 - \frac{U_p}{U_{p\max}}) \tag{17}$$

Where,

$$U_p = \sum \left| \Delta U_p \right| \tag{18}$$

3. Experimental tests

3.1 Single-edge notched beam test

Figure 4 llustrates a simply-supported, single-edged notched beam (SE(B)) with a length of 376 mm, a height of 100 mm and a thickness of 75 mm. A notch was then inserted with a length of 19 mm, giving a notch to depth (*a/H*) ratio of 0.19. The depth of the notch was selected to be long enough to ensure adequate stress intensity at the notch tip to initiate a crack, but short enough to ensure a ligament of adequate length for test repeatability and to prevent crack initiation under self-weight. The constant crack mouth opening displacement (CMOD) loading rate, 0.7 mm/min, is imposed at the center of the top edge of the specimen in order to predict stable fracture behavior. As shown in Figure 4, a clip-on gauge with a range of 6.35 mm was used for measuring the CMOD. The CMOD gage was attached to the beam using gage points that were glued to the edge of the notch. The test was conducted in a temperature controlled environmental chamber capable of maintaining air temperature within ±0.2 °C.

Figure 4 SE(B) geometry and test configuration

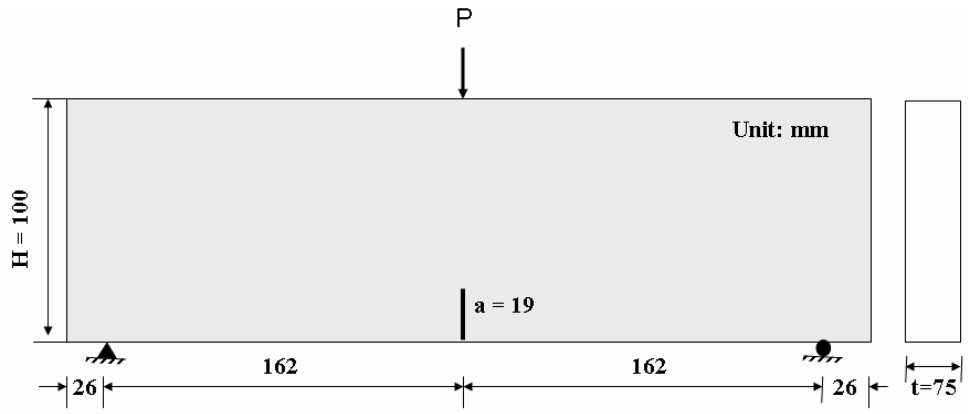

(a) SE(B) Test Geometry

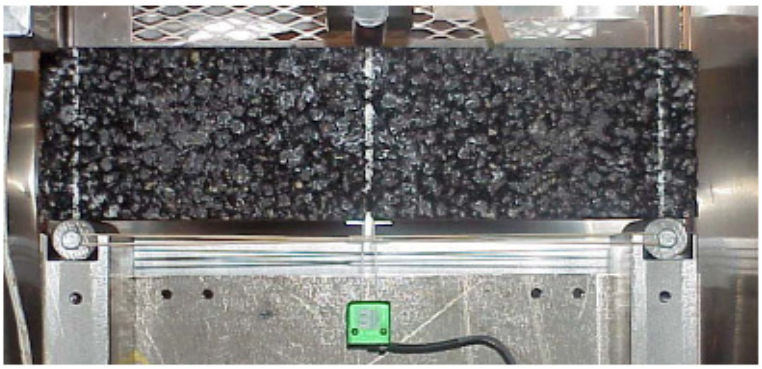

(b) Test Configuration and Clip-on Gage

3.2 Disk-shaped compact tension test

The main purpose for the development of the disk-shaped compact tension (DC(T)) test specimen geometry was the ability to test cylindrical cores obtained from in-place asphalt concrete pavements and gyratory-compacted specimens fabricated during the asphalt concrete mixture design process for relevant fracture properties. The dimensions of the specimen were determined by using the ASTM E399 Standard as a guideline. As shown in Figure 5(a) and Table 1, the specimen diameter is 150mm and both cored hole diameters within the specimen are 25mm. The width of the specimen (W) was 110 mm with the notch length (a) being 27.5 mm (a/W = 0.25). Therefore, the initial ligament length (W-a) was 82.5 mm. The thickness (t) of the specimen was 50 mm. The dimensions noted in the figure were initially developed for 9.5 mm NMAS mixtures, but has been successfully applied to 4.75 mm and 19 mm NMAS mixtures. Figure 5(b) shows DC(T) test configuration and clip-on gage. The DC(T) test is loaded in tension through the loading holes and is conducted with a constant CMOD rate of 1 mm/min.

Figure 5 DC (T) Specimen Geometry for Asphalt Concrete

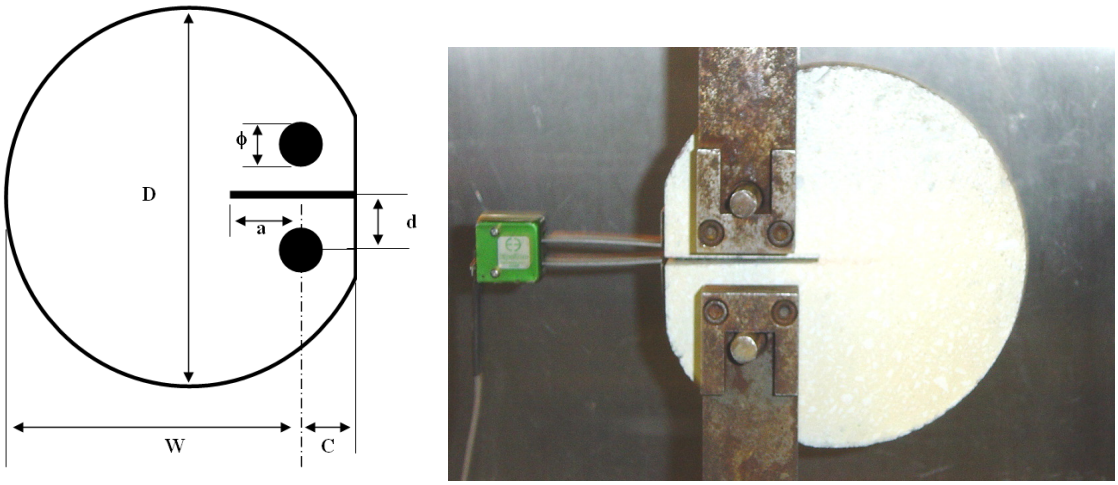

(a) DC (T) Specimen Geometry (b) DC(T) Test Configuration and Clip-on Gage

Table 1 DC(T) Dimension

Dimension	mm
D	150
W	110
a	27.5
d	25
C	35
Φ	25
t	50

4. Material properties and image analysis

Two different mixtures (LR-19 and LR-9.5) were used with the same aggregate type (dolomite limestone) from a local central Illinois source in USA. The materials used herein are asphalt mixtures with 9.5mm and 19mm nominal maximum aggregate size (NMAS). The aggregate gradation plot is shown in Figure 6. PG64-22 binder was used for both mixtures.

Figure 6 Aggregate gradations of asphalt mixtures with 9.5 mm NMAS

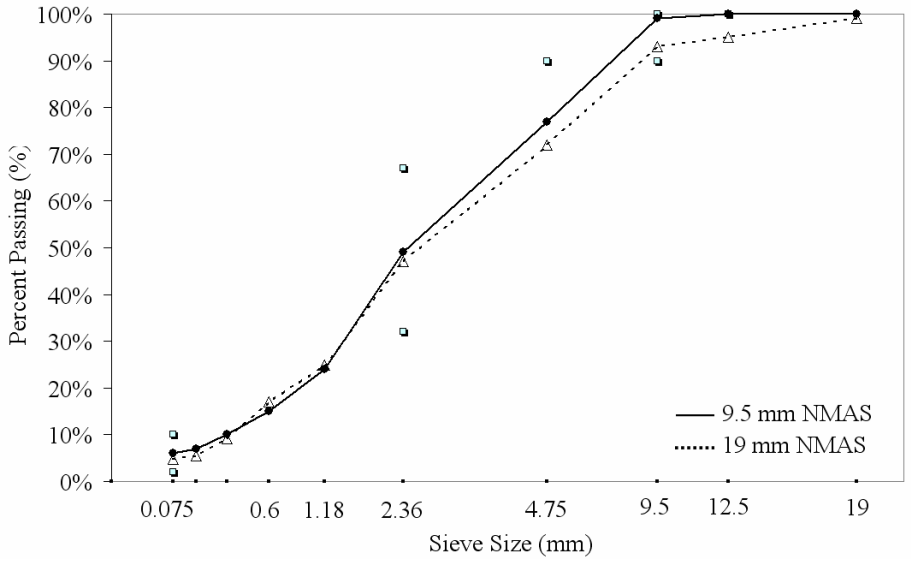

One of the important procedures to make a heterogeneous fracture model is the image processing to capture the real microstructure using high-resolution image scanning (Resolution: 1600×1600, Pixel size: 0.016 mm) and user-defined program, which can detect aggregate locations and shapes in asphalt mixtures. As illustrated in Figure 7 and Figure 8, a digital image can be obtained from the specimen via scanning and projected onto a discrete element mesh using Image-Pro Plus (Media Cybernetics, 2004) and a user-defined Excel VBA program. Next, the holes which facilitate loading pins and the mechanical notch are simulated by removing appropriate elements in the simulated specimen. DC(T) DEM specimens which capture the sand-size (0.3 mm) and larger aggregate features of 19mm nominal maximum aggregate size (NMAS) mixtures can be obtained with this technique. Also, some of important information such as each aggregate area, aspect ratio, diameter and perimeter, aggregate angle, and roundness can be obtained and analyzed to investigate the sensitivity of microstructure on the fracture process.

Figure 7 Image projection procedure of microstructure into DEM mesh

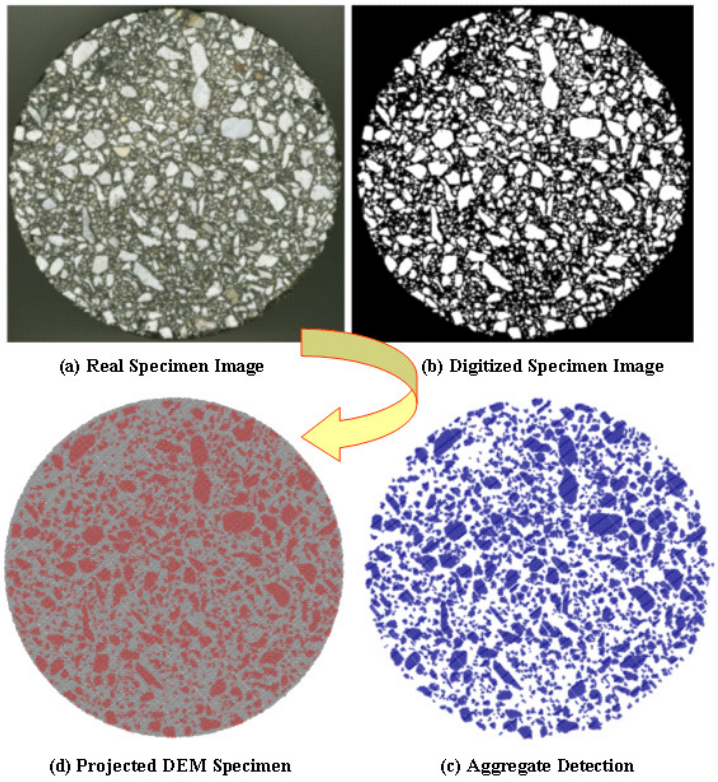

Figure 8 Numerical and laboratory DC(T) specimen images

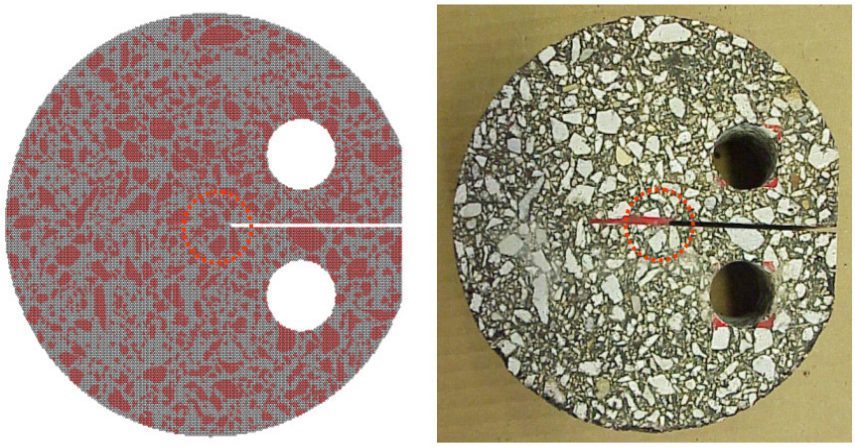

(a) DEM Specimen Representation (Left) and Laboratory Specimen (Right)

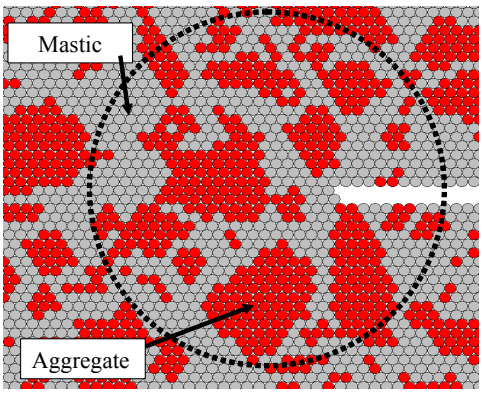

(b) DEM mesh around a notched crack tip

Figure 9 schematically illustrates modeling approaches used for the heterogeneous cohesive fracture investigation using PFC-2D. The asphalt concrete specimen was divided into three phases: aggregate, mastic, and interface between aggregate and mastic. For the material fracture properties, it was assumed that each phase has a material fracture behavior such as linear elastic for aggregate, bilinear elasto-plastic for mastic, and bilinear elasto-plastic for interface because of the softening of one side mastic. But the softening displacement of interface is much smaller than that of mastic (Ince et al., 2003). As illustrated in Figure 9, each phase requires an independent set of material parameters namely: Young's modulus; tensile strength, and fracture energy. Current experimental procedures limit the ability to measure all of the required parameters, especially the interface parameters. A limited number of experiments conducted on the aggregates, mastics, and mixtures, combined with typical values obtained in the literature (Tschegg et al., 1995) allowed for the determination of most material parameters (i.e., Young's modulus, tensile strength, and fracture energy for both aggregate and mastic). For the remaining parameters (i.e., tensile strength and fracture energy for the interface between aggregate and mastic), calibration procedure was used to estimate from assumed seed values. A sensitivity analysis was conducted to determine the effect of the interfacial properties on the global fracture response. The goal of the sensitivity analysis was not necessarily to match experimental results but rather to develop the understanding of the effects of the interfacial properties. The details of sensitive analyses are beyond the scope of this paper but can be found in author's publications (Kim et al., 2008(a)).

Figure 9 Multi-phase DEM geometries and assumed material properties

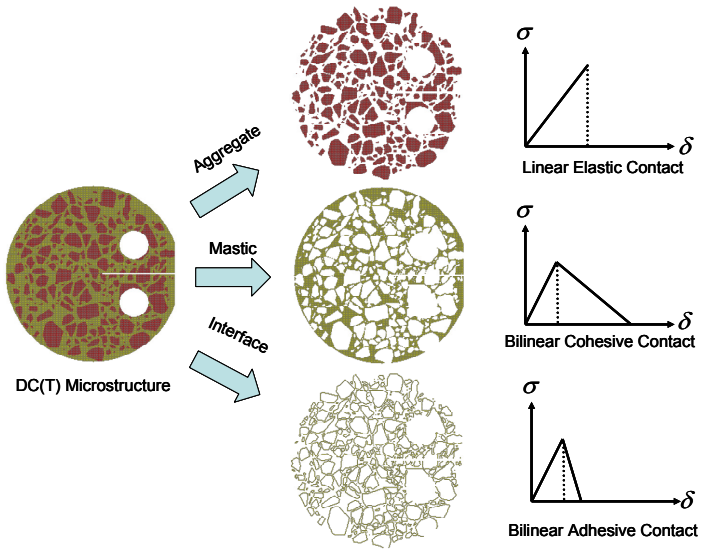

5. Numerical results

5.1 Heterogeneous SE(B) modeling

Figure 10 represents the numerical heterogeneous model geometry and crack propagation results. In this model, 149,922 particles with 0.25mm radius and 298,855 contacts are used across the entire specimen and 61,717 particles and 105,236 contacts are used to model aggregates; 88,205 particles and 158,042 contacts for mastic, and; 35,577 contacts are used at the interfaces between aggregate and mastic sub-particles (Kim et al., 2008(b)). The material parameters of aggregate and mastic were obtained from indirect tension (IDT) and dynamic modulus tests (You, 2004). The material parameters of interface were assumed that they are similar to the mastic. The fracture energies of mastic and interface were estimated and calibrated based on the experimental fracture test data of mixture. The stress concentration in the ligament along the expected mode I crack path is significant and many micro-cracks were predicted in the process zone prior to crack propagation, as shown in Figure 10. Figure 10(b) show many micro-cracks around an aggregate in the top of notched crack tip. From the experimental tests and numerical simulations, the powerful potential benefits of DEM fracture model can be discussed. The fracture of asphalt concrete has very different fracture mechanisms due to the non-homogeneity in the specimen such as micro-cracking, crack branching and deflection, crack face sliding, crack bridging, and crack tip blunting. The micro-cracking phenomenon consumes a part of the external energy caused by the applied load. Crack deflection occurs when the path of least resistance is around a relatively strong particle or along a weak interface. Also, during the opening of a tortuous crack, there must be some frictional sliding between the cracked faces that causes energy dissipation through friction. Based on these mechanisms in the fracture of asphalt concrete, heterogeneous DEM fracture model can have the ability to gain some insight towards fracture toughening mechanisms in asphalt concrete.

Figure 10 Heterogeneous DEM fracture model and representations of cracks

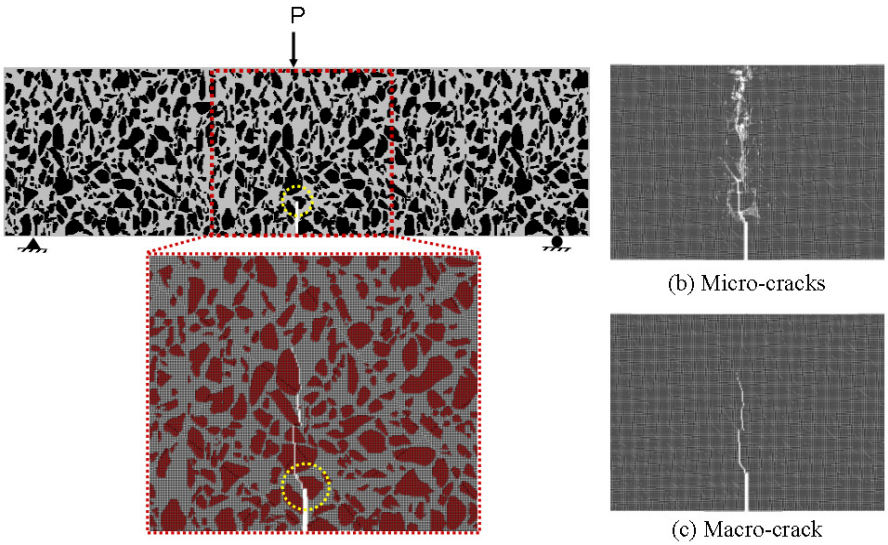

For the calibrated heterogeneous fracture simulation, the overall trend resembled the experimental result as shown in Figure 11. Due to the presence of a large aggregate just ahead of the simulated notch, the force was predicted to experience a sudden decrease before the peak load but then was recovered. This phenomenon has been observed in experimental trials, particularly when thin specimens with larger aggregates are tested. Thus, the 2D model herein tends to exaggerate the effect of aggregates on the load-CMOD response, especially when compared to experimental results obtained from specimens with larger thicknesses-to-maximum-aggregate size ratios. Thus, the need for three-dimensional modeling to accurately capture material heterogeneity is apparent.

Figure 11 Experimental and numerical responses (9.5mm NMAS at -10 °C)

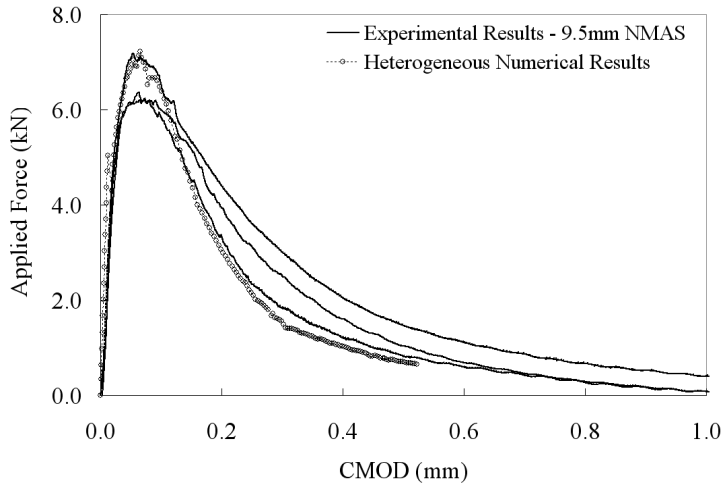

The mixed-mode fracture in a pavement system is popular and significant due to the presence of continuous dynamic and static traffic loads and environmental conditions including temperature and moisture. Using the calibrated cohesive parameters and particle size 0.25mm, the mixed-mode problem was investigated herein using the SE(B) test with an offset notch to create mixed-mode (i.e., mixed with Mode-I and Mode-II) crack propagation. The shear parameters of fracture properties were the same with normal parameters. The offset parameters, γ, as defined in Figure12, were 0.4, 0.5, and 0.55 resulting in offset lengths of 65 mm, 81 mm, and 89 mm from the middle of specimen.

Figure 12 Mixed-mode SE(B) geometry with offset notch

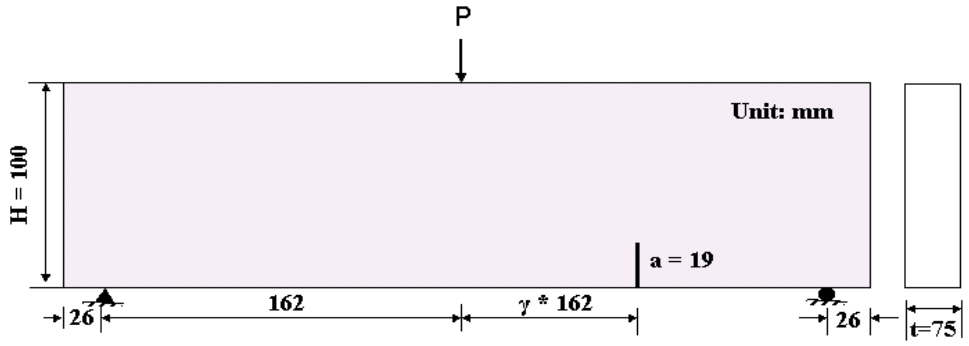

Figure 13 shows the crack paths for the three beams, plus the standard SE(B) beam (γ = 0). Based on the test results, the critical offset was between γ =0.5 and 0.55. Although only one material was tested, the critical offset should depend on the material toughness and also on the notch depth. Therefore, the study should be extended to investigate different materials and notch lengths to provide a full experimental investigation. Figure 13(b) shows the numerical failed beams with 0.55 notch offset and the crack propagation was progressed from the middle of the specimen.

Figure 13 Experimental and numerical trajectories path with various notch offsets

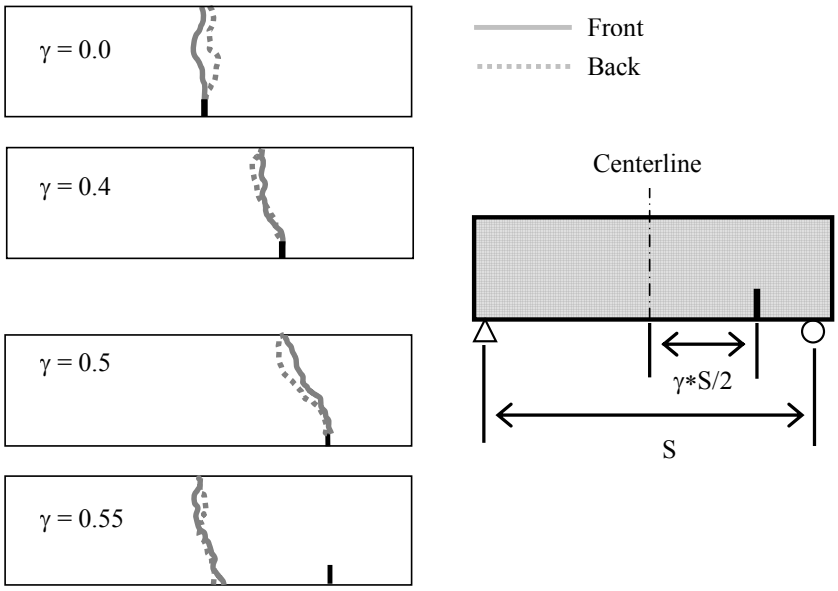

(a) Experimental crack trajectories

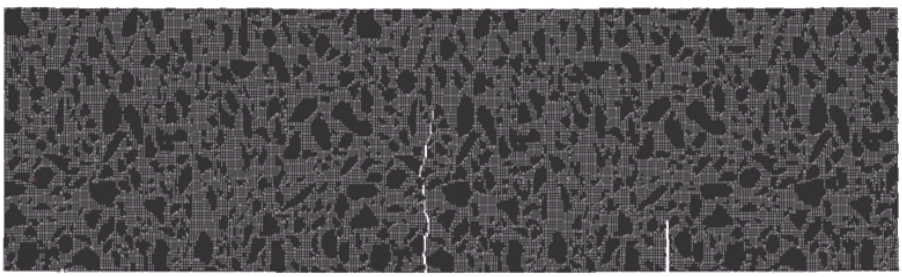

(b) Numerical crack trajectories (γ = 0.55)

For the beam with 0.4 notch offset, the macro-crack initiated with mode-I fracturing in but the path quickly began to meander at an angle towards the loading point as the crack propagated. Before crack initiation, inelastic effects at the crack tip in the notched region and in the vicinity of the outer fiber of bending at the bottom of the mid-span of specimen are simultaneously occurring (Figure 14).

Figure 14 Progressive crack initiation and propagation by numerical model ($\gamma = 0.4$)

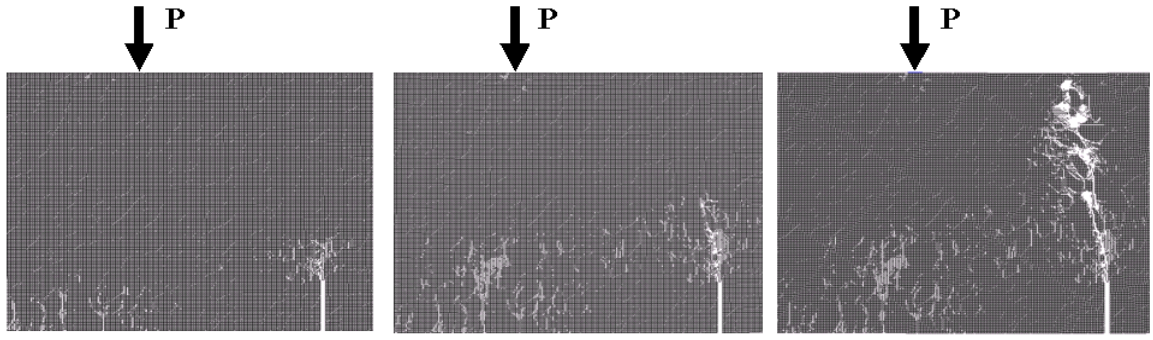

(a) Micro-Crack Initiation (b) Macro-Crack Initiation (c) Crack Propagation

5.2 Heterogeneous DC(T) modeling

Heterogeneous DC(T) fracture simulations were done to verify the SE(B) results if the predicted material parameters could be fitted into different test modes. The heterogeneous cohesive fracture simulation of a 19mm NMAS mixture was comprised of a total of 38,721 discrete elements, each having 0.35mm radius forming 114,994 contacts in the horizontal hexagonal packing arrangement. For the clustered DEM technique used in this study, the microstructure was mapped upon a uniformly generated sheet of hexagonally arranged circular elements. The diameter of the discrete element was carefully selected so that irregular geometrical features, such as aggregates, can be modeled by bonding a number of elements together and assigning the proper material properties within the bonded clusters and at the interface between aggregates and mastic. Various fracture mechanism related to temperature and microstructure could be investigated by heterogeneous DEM fracture models (Kim and Buttlar, 2005).

Figure 15 Comparisons of experimental and numerical results at different temperatures

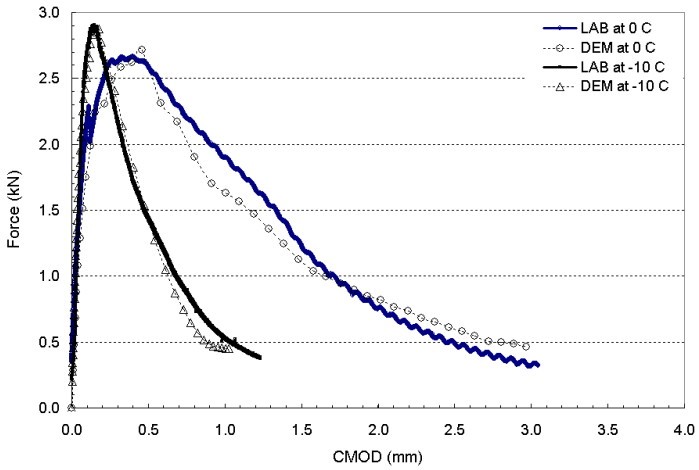

(a) Force vs. CMOD Curves at Different Temperatures

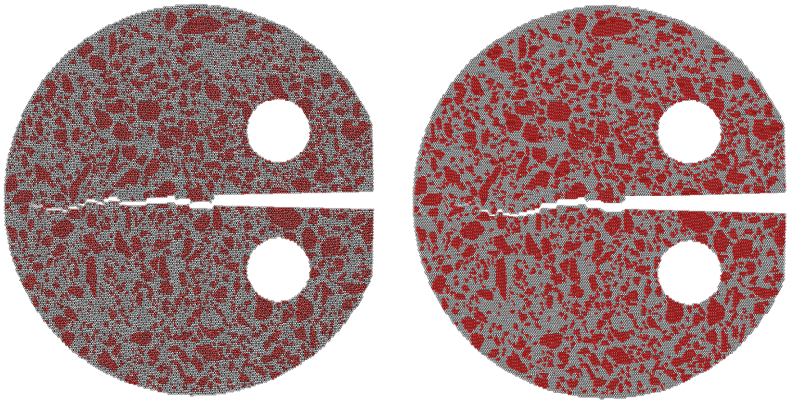

(b) Crack Trajectory at -10 °C (c) Crack Trajectory at 0 °C

Table 2 Heterogeneous DEM model parameters at different temperatures

9.5 mm NMAS		Material Properties		DEM Contact Properties	
Temperature (°C)	Phase	Young's Modulus (GPa)	Tensile Strength (MPa)	Stiffness (GPa)	Bond Strength (MPa)
-10°C (B: 54mm)	Aggregate	56.8	6.59	2.9	169

	Mastic	14.2	3.0	0.77	82
	Interface	14.2	2.8	0.77	74
	Aggregate	56.8	6.59	2.9	169
0°C (B: 51mm)	Mastic	9.9	2.7	0.51	69
	Interface	9.9	2.5	0.51	63

Using more successful aforementioned image analysis, numerical simulations with the same microstructure as experimental specimens were compared. Figure 16 and Figure 17 compare the experimental and numerical results including crack path and trajectories, force vs. CMOD curves, micro-cracks, and stress concentration in the fracture process zone area. The micro-cracking of the DEM model occurred when the softening starts in the local model after passing the material strength.

Figure 16 Crack trajectories and force vs. CMOD curves (19mm NMAS)

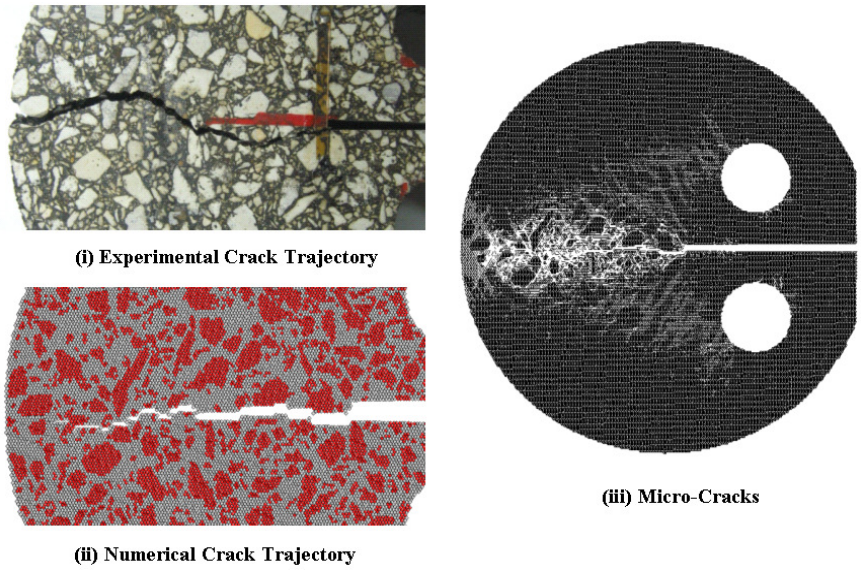

(a) A Comparison of Crack Trajectories and Micro-Cracks

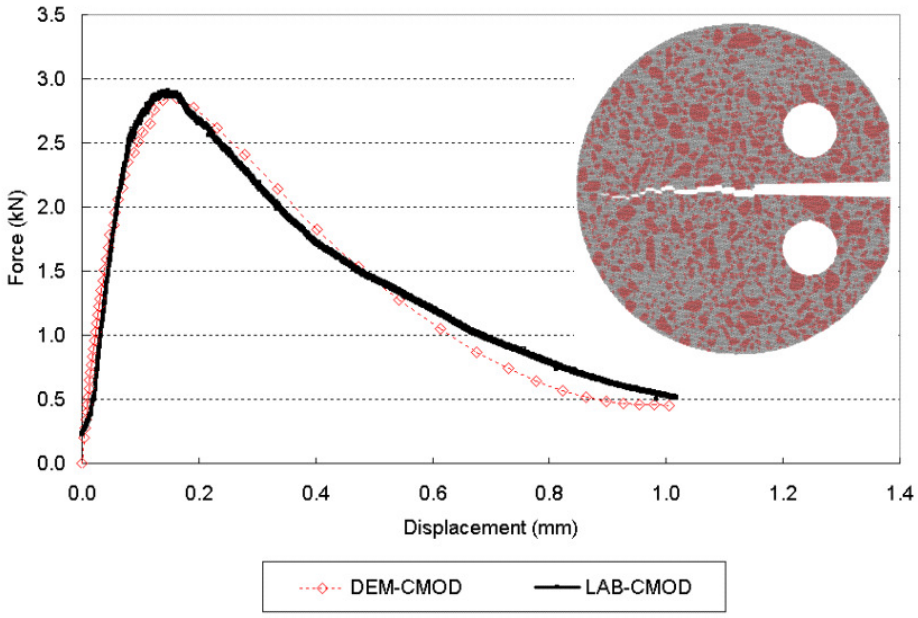

(b) Comparisons of Experimental and Numerical Results

Figure 17 Crack trajectories and force vs. CMOD curves (9.5mm NMAS)

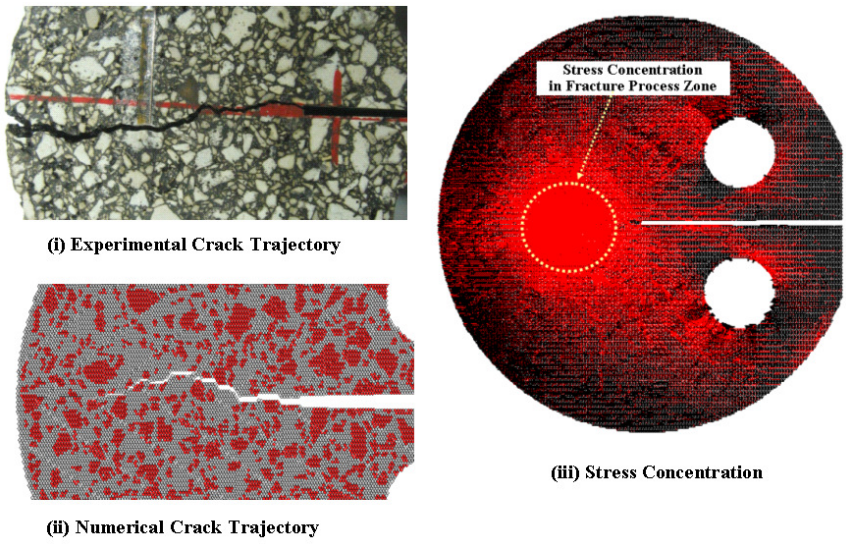

(a) A Comparison of Crack Trajectories and Stress Concentration

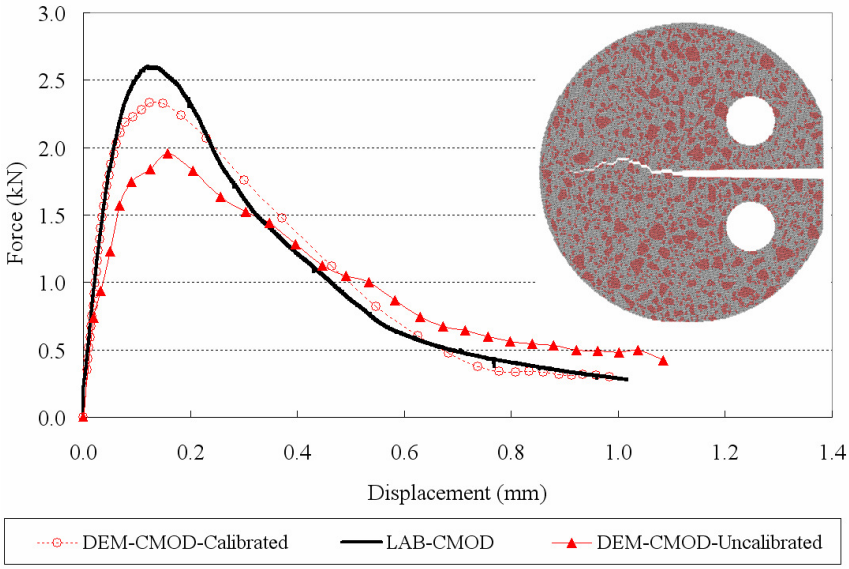

(b) Comparisons of Experimental and Numerical Results

An important finding from this exercise is that complete material separation just ahead of the mechanical notch in the 150 mm diameter DC(T) specimen occurs only after peak load is reached in the experiment. This suggests that the fracture process zone (FPZ) is relatively large as compared to specimen dimensions, suggesting that linear elastic fracture mechanics principles should not be expected to hold for HMA. The FPZ is a nonlinear zone characterized by progressive softening, where the traction across the forming crack surface decreases as separation increases. The different fracture toughening mechanisms of brittle, quasi-brittle, and ductile materials are greatly influenced by the characteristics of the FPZ. Since the FPZ consumes a substantial amount of the energy supplied by the applied load, the presence of the fracture process zone is important for the fracture response after the peak load is reached. To study this phenomenon in more detail, the extent of the zones of compression, tension, softening and fracture in the DC(T) specimen as a function of CMOD (and thus time) were obtained from the DEM simulations. As shown in Figure 18, the extent of the softening zone increased until well after crack initiation and then gradually decreased as the crack propagated. Clearly, the softening zone size is affected by proximity to the specimen boundary, due mainly to the flexure present in the DC(T) test, not unlike that present in bending tests. Once again, the size of the fracture process zone is far from negligible, since at times during the test it encompasses more than half of the eventual fracture ligament.

Figure 18 Numerical progressive fracture process (19mm NMAS at -10 °C)

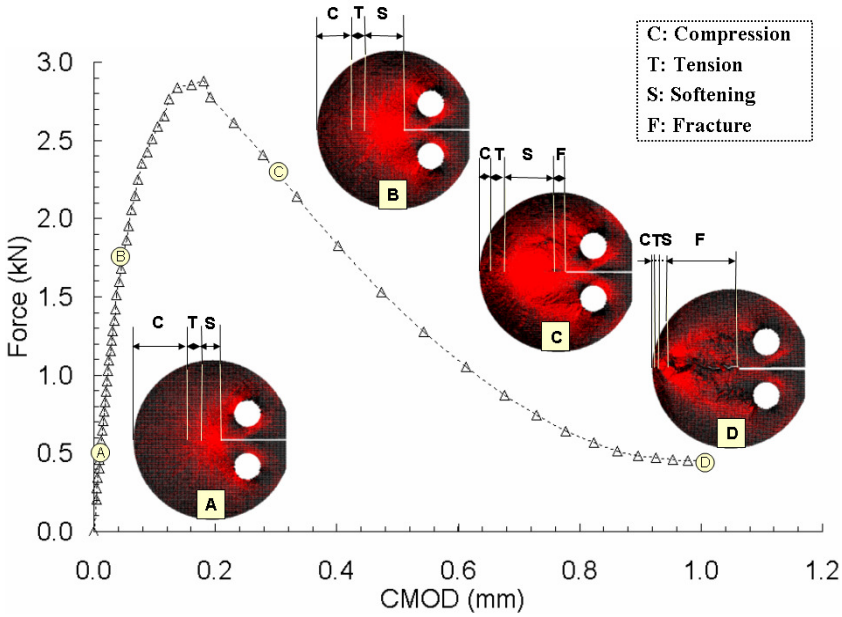

6. Conclusions and discussions

A micromechanical fracture modeling approach has been employed to investigate various toughening mechanism in the fracture of asphalt concrete. Using a high-resolution image technique, the microstructure of asphalt mixture was obtained and directly considered in the fracture modeling approach. Mode-I and mixed-mode fracture models were implemented, simulated, and compared with experimental (DC(T) and SE(B)) test data to validate the numerical results and to determine the material parameters using calibration procedure. Numerical results matched well with experimental results, even in cases where different test modes were simulated using the same multi-phase material parameters.

The heterogeneous fracture simulation demonstrated the potential usefulness of the approach in the investigation of fracture mechanisms in asphalt concrete. A near-term application of the discrete element modeling techniques presented is the ability to simulate several laboratory tests, such as creep, stiffness, strength, and fracture, with essentially the same material 'fabric'. The simulation of numerous laboratory tests can be used to reduce the amount of expensive and time-consuming experimental tests required for mechanistic-empirical design and analysis programs. Some of works related to the specimen size dependency and the rate-dependent fracture behavior were already done and have been continuously investigating (Kim et al., 2009(a) and Kim et el., 2009(b)). Future work in areas such as three-dimensional (3-D) image analysis using the x-ray tomography (Partl et al., 2003), 3-D heterogeneous modeling; large-scale, e.g. pavement system modeling; experimental determination of interface material properties; systematic or statistical modeling of material defects and air voids; dynamic fracture modeling will lead to even more powerful modeling capabilities.

7. References

Barenblatt, G.I. (1962) Mathematical theory of equilibrium cracks in brittle fracture, *Advances in Applied Mechanics*, Vol. 7, pp. 55-129.

Cundall, P. A. (1971) A computer model for simulating progressive, large-scale movements in blocky rock systems, *Proceedings of the International Symposium of Rock Fracture*, Nancy, France, paper no. II-8.

Dugdale, D. (1960) Yielding of steel sheets containing slits, *Journal of Mechanics and Physics of Solids*, Vol. 8, pp. 100-104.

Geubelle, P. H. and J.S. Baylor (1998) Impact-induced delamination of composites: a 2D simulation", *Composites Part B*, 29B, 589-602.

Hillerborg, A., M. Modeer, and P.E. Petersson (1976) Analysis of crack formation and crack growth in concrete by means of fracture mechanics and finite elements, *Cement and Concrete Research*, Vol. 6, No. 6, pp. 773-782, Nov.

Ince, R., A. Arslan, and B.L. Karihaloo (2003) Lattice modeling of size effect in concrete strength, *Engineering Fracture Mechanics*, Vol. 70, 2307-2320.

ITASCA Consulting Group, Inc. (2002) *PFC 2D version 3.0*, Minneapolis, Minnesota 55415, USA.

Kim, H. and W.G. Buttlar (2005) Micromechanical fracture modeling of hot-mix asphalt concrete based on a disk-shaped compact tension test", *Journal of the Association of Asphalt Paving Technologists*, Volume 74E.

Kim, H., M.P. Wagoner, and W.G. Buttlar (2008(a)) Simulation of heterogeneous cohesive fracture model in asphalt concrete using discrete element method, *Journal of Materials in Civil Engineering*, Vol. 20, No. 8, pp.552-563.

Kim, H., M.P. Wagoner, and W.G. Buttlar (2008(b)) Experimental and numerical prediction of fracture behavior of asphalt mixture using single-edge notched beam test, *Materials and Structures*, (In press).

Kim, H., M. P. Wagoner, and W.G. Buttlar (2009(a)) Numerical fracture analysis on the specimen size dependency of asphalt concrete using a cohesive softening model, *Construction and Building Materials*, (In press).

Kim, H., M.P. Wagoner, and W.G. Buttlar (2009(b)) Rate-dependent fracture modeling of asphalt concrete using the discrete element method, *Canadian Journal of Civil Engineering*, (In press).

Partl, M.N., A. Flisch, and M. Jönsson (2003) Gyratory compaction analysis with computer tomography, Road Materials and Pavement Design, Vol.4(4), pp.401-422.

Media Cybernetics Inc. (2004) *Image-Pro Plus 5.0*, Silver Spring, Maryland, USA.

O'Sullivan, C. and J.D. Bray (2001) A comparative evaluation of two approaches to discrete element modeling of particulate media, *Proceedings of the Fourth International Conference on Discontinuous Deformation*, pp.97-100, University of Glasgow, Scotland, UK.

Tschegg, E.K., H.M. Rotter, P.E. Roelfstra, U. Bourgund, and P. Jussel (1995) Fracture mechanical behavior of aggregate – cement matrix interfaces, *Journal of Materials in Civil Engineering*, Vol. 9, No. 4, pp.199-203.

You, Z. and W.G. Buttlar (2005) Discrete element modeling to predict the modulus of asphalt concrete mixtures, *ASCE Journal of Materials in Civil Engineering,* Vol. 17, pp. 140-146.